

**СООБЩЕНИЯ
ОБЪЕДИНЕННОГО
ИНСТИТУТА
ЯДЕРНЫХ
ИССЛЕДОВАНИЙ
ДУБНА**

E7-84-415

M.Biedermann*, P.Mädler, R.Reif*

**TDHF-MOTIVATED MACROSCOPIC MODEL
FOR HEAVY ION COLLISIONS:
A COMPARATIVE STUDY**

* Technische Universität Dresden, Sektion Physik,
8027 Dresden, DDR

1984

1. INTRODUCTION

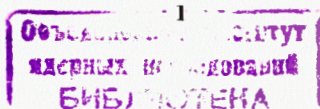
Recently G.F. Bertsch proposed a classical heavy ion collision model which mimics the dynamics of time-dependent Hartree-Fock theory (TDHF)^{/1/}.

In this model, in addition to the relative coordinate r of the centers of mass of the two nuclei, only one more geometric variable, the radius r_{neck} of a neck joining the nuclei, is considered. The acceleration of the relative coordinate is macroscopically given by the sum of a Coulomb force, a bulk nuclear force, and a surface tension:

$$\mu \ddot{\vec{r}} = \vec{F}_{\text{Coul}} + \vec{F}_{\text{bulk}} + \vec{F}_{\text{surface}} \quad (1)$$

with μ being the reduced mass of the nuclei. These forces are expressed solely in terms of r and r_{neck} . For the evolution of r_{neck} a simple model was set up, based on the results of realistic TDHF calculations. Since the TDHF-neck dynamics is quite different, in the approach and rebound phases not only the bulk nuclear force in eq. (1) (nucleon flux across the neck) but also \vec{F}_{surface} essentially contribute to energy loss. Roughly half of the total kinetic energy loss (TKEL) can be related to the energy cost of stretching out the fused nuclei into an extended system with a long neck^{/1/}. The later stage of conversion of deformation energy into intrinsic motion of the separated fragments is not considered in this model since it obviously does not influence trajectories, TKEL, deflection functions and other quantities which can be calculated in TDHF. The question of whether the inclusion of residual nucleon-nucleon interactions into TDHF prevents large dynamical deformations in the final stage of the collision process by rapidly converting them into heat is, therefore, out of discussion as long as one is not concerned with particle emission which is very sensitive to the nature of the excitation.

A first comparison of this model with some TDHF-results and experimental data indicates that the main features of TDHF are well reproduced^{/1/}.



In the present paper we aim to get a more detailed insight into the dynamics of this model, and to test it against recent TDHF results as well as other model predictions.

2. THE MODEL

In this section we briefly describe the model under consideration, closely following ref. ^{/1/}.

We start with the specification of the three forces entering eq. (1).

The surface force is just the surface tension σ multiplied by the circumference of the neck:

$$\vec{F}_{\text{surface}} = r_{\text{neck}} \cdot 2\pi \sigma \frac{\vec{r}}{r} . \quad (2)$$

A value of $\sigma = 1.0 \text{ MeV/fm}^2$ taken from the empirical surface energy is used.

The bulk nuclear force is assumed to be described by the window formula ^{/2/}, i.e., its tangential and longitudinal components are:

$$F_T = -\frac{dn}{dt} m v_T^N , \quad F_L = -\frac{2dn}{dt} m v_L^N , \quad (3)$$

where

$$\frac{dn}{dt} = \frac{3}{16} S_0 v_F \pi r_{\text{neck}}^2 \quad (4)$$

is the one-sided flux of particles across the surface, evaluated in the Fermi gas model, $S_0 \approx 0.16 \text{ fm}^{-3}$ is the nuclear matter density, and $v_F \approx 0.28 c$ is the Fermi velocity. The quantities v_T^N and v_L^N are the relative tangential and longitudinal velocities of the Fermi surfaces on the two sides of the neck. Taking into account internal angular momentum ℓ_i of the nuclei ($i=a,b$) v_T^N is defined by

$$v_T^N = \dot{r}_T - \frac{R_a \ell_a}{I_a} - \frac{R_b \ell_b}{I_b} . \quad (5)$$

Here r_T denotes the tangential component of the relative velocity \vec{r} , I_i and $R_i = 1.15 A_i^{1/3}$ are the moment of inertia and the nuclear density radius of nucleus i . Assuming that the torque on a nucleus is proportional to its radius, from angular momentum conservation follows

$$\ell_i = (\ell_{i,\text{initial}} - \mu r \dot{r}_T) R_i / (R_a + R_b) . \quad (6)$$

The moments of inertia in eq. (5) are taken to be those of ellipsoids with axes R_i and $rR_i/(R_a+R_b)$.

In eq. (3) the relative longitudinal velocity of the two Fermi spheres v_L^N is not simply taken to be equal to the longitudinal

component \dot{r}_L of the center-of-mass motion (as it has been assumed in ^{/2/}). Namely, the shape of the Fermi surface at the neck position is determined by the velocities of the nuclear surfaces at some earlier time, when the nucleons that have reached the neck region were being reflected from distant surfaces ^{/3/}. This time delay is approximately taken into account by determining $v_L^N(t)$ from the relation

$$\frac{m}{2} (v_L^N(t) - v_F)^2 = \frac{m}{2} (v_D - v_F)^2 + \frac{Z_a Z_b e^2}{A_a} \left[\frac{1}{\lambda r(t) + R_a} - \frac{1}{\lambda r(t)} \right] \quad (7)$$

with

$$v_D = \dot{r}_L(t - t_D) \cos(\Delta\varphi) + \dot{r}_T(t) \sin(\Delta\varphi) , \\ \Delta\varphi = \arctan[\dot{r}_T(t) t_0 / r(t)] , \\ t_0 = \frac{2R_a}{v_F} , \quad \lambda = \frac{R_b}{(R_a + R_b)} .$$

The second term in the r.h.s. of eq. (7) describes the slowing down of the nucleons in traversing the nucleus due to the long range of the Coulomb force. The time scale of the time delay t_D is set by the transit time t_0 (a is taken to be the smaller nucleus). In ref. ^{/1/} a standard value of

$$t_D = 1.5 t_0 \quad (8)$$

has been chosen.

The Coulomb force in the approach phase (where the neck plays a minor role) as well as in the first stage of the rebound phase (as long as $s = r - R_a - R_b < 0$) is taken to be that of two point charges at distance r . In the final stage, for $s > 0$, the system is treated as two spheres joined by a cylinder, whose radius is r_{neck} and length is s . Then, the Coulomb force is approximated by

$$F_{\text{Coul}} \approx e^2 \left[\frac{(Z_a - Z_n)(Z_b - Z_n)}{(r_a + r_b)^2} + \frac{(Z_a - Z_n)Z_n}{(r_a + \frac{s}{2})^2} + \frac{(Z_b - Z_n)Z_n}{(r_b + \frac{s}{2})^2} + \frac{Z_n^2}{(\frac{s}{4} + \frac{r_{\text{neck}}}{2})^2} \right] \quad (9)$$

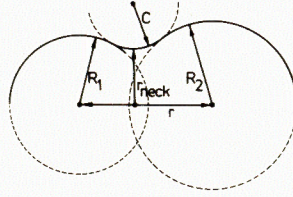
with

$$Z_n = \pi r_{\text{neck}}^2 S_z \frac{s}{2} , \quad S_z \approx \frac{S_0}{2}$$

$$r_{a,b} = \frac{Z_{b,a} (R_{b,a} + \frac{s}{2}) - Z_n \frac{s}{2}}{Z_{b,a} - Z_n} .$$

Finally, to accurately describe grazing collisions, the Bass potential ^{/4/} is included in the model before the nuclei touch and form a neck. There is also particle transfer at large distances due to nucleon tunnelling under the potential barrier. For the corresponding tunnelling rate dn/dt the static parametrization of ref. ^{/5/} is adopted assuming that this particle flux carries the same momentum as in eq. (3).

Fig.1. Geometry of the Bertsch model.



The geometry of the model is that of three touching circles representing the two nuclei and a joining neck. From Fig. 1 a simple geometrical relation can be deduced connecting r_{neck} with R_1 , $r(t)$ and $c(t)$:

$$r_{neck} = \sqrt{\frac{(R_a + R_b + r + 2c)(R_a + R_b - r + 2c)(r + R_a - R_b)(R_b + r - R_a)}{2r}} - c. \quad (10)$$

In the approach phase it is assumed that the growth in c is a highly overdamped process; so the rate at which it changes is proportional to the force associated with that coordinate. Hence,

$$\dot{c} = \alpha / c. \quad (11)$$

The rebound phase has completely different dynamics. It is several times as long as the approach phase, so hydrodynamical considerations are more likely to be relevant in describing the overall shape. Again, it is assumed that the motion is overdamped, and that the force responsible for the neck shrinkage is proportional to r_L

$$\dot{r}_{neck} = -\beta \dot{r}_L. \quad (12)$$

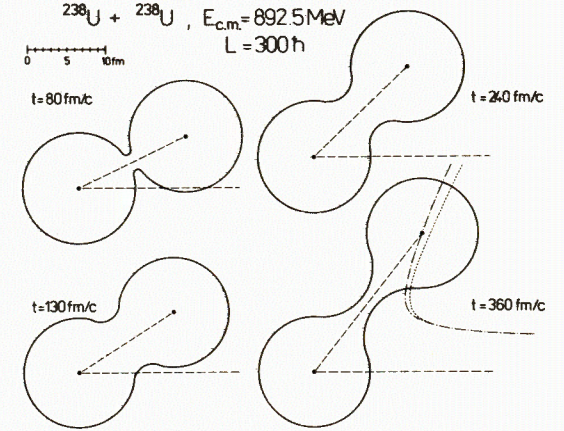
The parameters α and β of eq. (11) and (12) are fitted to TDHF results of ref.^{/6/} and used as standard values ($\alpha = 0.04$ fm/c, $\beta = 1/3$). With these parameters the results of ^{/6/} are convincingly well reproduced by eq. (11) and (12).

In accordance with the TDHF results of ^{/6/} the onset of the neck is assumed to occur with a small time delay of 9 fm/c after the potential radii R_i ($R_i = 1.25 A^{1/3}$) touch. This defines initial conditions for eqs (11), (12).

Scission is treated in the model as the neck becoming hydrodynamically unstable if it is too narrow in relation to its length^{/11/}. It is assumed that scission occurs suddenly when $r_{neck} \leq 1$ fm.

Another mechanism for neck breakage is when the nuclei rebound at high velocity. An instability develops with respect to density fluctuations when the bulk density falls below about $2/3 \rho_0$. This separation mechanism, called "neck snapping", is shown ^{/18/} to occur in mean field theory for r_L or V_L exceeding a value of 0.06 c.

Fig.2. Time evolution of the shape of two colliding ^{238}U ions. The mass center of one of the ions is fixed. Dotted line: pure Coulomb trajectory. Dotted-dashed line: trajectory calculated in the Bertsch model.



For a given energy and impact parameter the system is considered to be fused if in the rebound phase the rebound velocity decreases to zero and becomes negative leading - as in TDHF - to subsequent cycles of oscillations in $r(t)$.

We complete this section with an illustration of some main qualitative features of the model dynamics.

Figure 2 shows the time evolution of the shape of two colliding ^{238}U ions at $E_{c.m.} = 892.5$ MeV, $L_{in} = 300$ h. The time is scaled from the instant where $r = 18.6$ fm (for larger r a pure Coulomb trajectory is used). At $t \approx 80$ fm/c the neck (9 fm/c after the potential radii touch) opens immediately acquiring a finite radius. This is connected with the choice of the initial value of c_0 as $c_0 = \max\{0.5 \cdot (r - R_a - R_b) + 0.1 \text{ fm}, 0.1 \text{ fm}\}$ used in the model. This somewhat arbitrary choice guarantees that the starting value of r_{neck} for any systems as it is defined from geometric relations eq.(10) remains positive. Furthermore, it is sufficiently small to have no significant physical consequences as compared to a zero starting value for r_{neck} . The turning point of the collision is reached for about $t = 130$ fm/c and is characterized by a quite short but thick neck. In the long rebound phase the neck is substantially stretched and scission in the above described sense occurs at $t \approx 360$ fm/c.

Next, in Fig. 3. for the $^{84}\text{Kr} + ^{209}\text{Bi}$ reaction at $E_{lab} = 600$ MeV, $L_{in} = 180$ h, the forces entering eq. (1) are displayed as functions of $r(t)$. The difference of F_{Coul} in the approach and rebound phases is just due to the use of eq. (9) in the latter for $S > 0$. At $r = r_{switch} \approx 12.5$ fm the neck appears. Just at this point several discontinuities in the forces arise. The first one is in the bulk force which is switched from the tunnelling contribution to the force

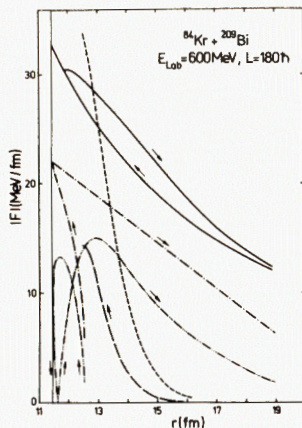


Fig. 3

The r - dependence of the forces entering eq.(1) for a Kr + Bi reaction. Full lines: Coulomb force. Dashed line: Bass force. Dotted-dashed line: surface force. Long-dashed line: friction force due to the tunnel flux. Three-dott-dashed line: friction force after opening of the neck.

only slightly influenced by the jump of the total force since for $r \approx r_{\text{switch}}$ the radial velocity (except for near-grazing collisions) is yet rather large so that the system quickly goes through the discontinuity.

3. CONTINUATION OF THE BULK FORCE

An improvement of the model leading to forces continuously changing from large to small distances would require a separate investigation which is not the object of the present work. However, we have found that some formal but not unphysical procedure of matching the bulk force at $r = r_{\text{switch}}$ "by hand" can give a considerable improve-

ment of the agreement with corresponding TDHF predictions. In this procedure we simply choose r_{neck} (and, correspondingly, c_0) in such a manner that F_{bulk} becomes continuous. Since r_{neck} enters the bulk force quadratically, only a small enlargement of r_{neck} is needed to yield the required effect (compare Fig.3). The surface force, being linear in r_{neck} , is also somewhat increased so that it comes closer to the Bass force. Due to the specific time dependence of c (eq.(11)) the values of F_{surface} and F_{bulk} at small distances near the turning point are only slightly enlarged compared to the standard version by about 5-10 %.

corresponding to the free flux, eq(4), through the neck, starting from a small non-zero value. The second one arises in replacing the Bass force by F_{surface} which also starts at a small non-zero value due to the choice of c_0 and, correspondingly, r_{neck} at $r = r_{\text{switch}}$ discussed above. The attractive surface force is clearly much stronger in the rebound phase than in the approach phase and, hence, it contributes to the energy loss. The memory effects approximately included in the radial friction force eq. (3) via $V_L^N(t)$ from eq.(7) can clearly be seen in the figure: F_{bulk} changes its sign (from repulsive to attractive) only about 0.15 fm after the turning point. In this region it helps to accelerate the rebounding ions, i.e., has some nondissipative part.

The discontinuities in the forces obviously are unphysical. They result from different physical inputs for large and small distances in the approach phase which are not sufficiently matched together. Fortunately, the two discontinuities enter the total force(1) with different sign and, therefore, partially cancel each other. Moreover, one usually looks for time-integrated quantities which are

only slightly influenced by the jump of the total force since for $r \approx r_{\text{switch}}$ the radial velocity (except for near-grazing collisions) is yet rather large so that the system quickly goes through the discontinuity.

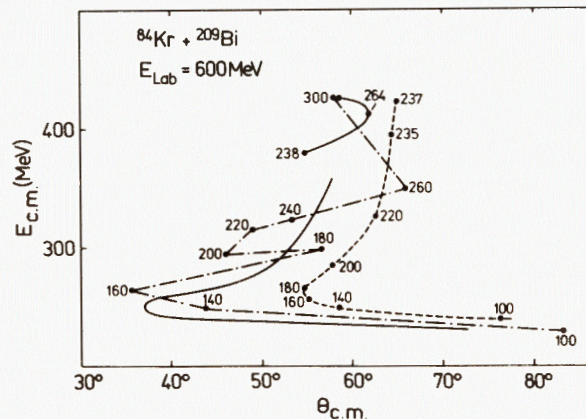


Fig. 4. Wilczynski plot for the Kr + Bi reaction at $E_{\text{lab}} = 600$ MeV. Dashed line: original Bertsch model. Full line: continuous bulk force (for details see text). Dotted-dashed lines: TDHF prediction taken from ref./9/. The numbers in the figure indicate the initial angular momentum in units of \hbar .

In order to demonstrate the effect of this procedure, in Fig.4 the Wilczynski plot for the reaction $^{84}\text{Kr} + ^{209}\text{Bi}$, $E_{\text{lab}} = 600$ MeV predicted by the model modified in the described manner is compared with the standard version as well as with TDHF /9/. The improvement of the agreement is substantial. The success is mainly connected with an effective enlargement of the neck radius at small distances. Since in ref./1/ it was found that the parametrization (11) and (12) somewhat underestimates the neck thickness at small distances, our formal procedure acquires some physical sense. In ref. /1/ nearly the same effect (for the same reaction) resulted after using a zero memory time t_D and reducing the Coulomb acceleration in eq.(7) by half. Although the dependence of the model results on (standard) input parameters should really be tested (see next section), this procedure seems to us to be much more artificial than the one described here.

The choice of r_{switch} at $t = 9 \text{ fm/c}$ after the potential radii touch was determined for a specific reaction considered in ^{16/} and used as a standard value in the model. Clearly, this is a further point which needs to be refined since for certain systems (higher energies) the tunnel flux becomes negative before $r = r_{\text{switch}}$ is reached. Correspondingly, there would be a short time interval in the approach phase with an accelerating bulk force. For example, this is the case for the $^{16}\text{O} + ^{93}\text{Nb}$, $E_{\text{lab}} = 204 \text{ MeV}$ reaction for which we have performed a model calculation and compared it with the TDHF results of ref. ^{10/}. Although the fusion region ($30 \text{ fm} \lesssim \ell \lesssim 75 \text{ fm}$) and the deep inelastic results for $\ell \gtrsim 75 \text{ fm}$ are close to TDHF, the deflection function and energy losses below $\ell = 30 \text{ fm}$ are in disagreement with TDHF. So, for $\ell \lesssim 30 \text{ fm}$ we found final c.m. energies around 130 MeV while TDHF predicts values around 30 MeV lying even below the Coulomb barrier in the entrance channel. We relate this to the acceleration effect of the bulk force mentioned above. Our procedure of continuation does not apply here since the fluxes would be matched at negative values. We applied a second version of continuation: redefine r_{switch} to be the point where the tunnel flux has its maximum and to determine r_{neck} at this point to get a continuous bulk force. This, however, gives a very large neck and consequently a very large friction. As a result, the fusion window vanishes completely, and in the vicinity of the fusion region it has been obtained orbiting.

As a third version the maximum value reached by the tunnel flux is used until the flux calculated from the neck geometry exceeds this value. In this case we could retain the agreement with TDHF for $\ell \gtrsim 30 \text{ fm}$ and came down to values around 65 MeV for the final c.m. energy in the region $\ell \lesssim 30 \text{ fm}$.

In Fig. 4 the discontinuity in going from $\ell = 238 \text{ fm}$ to lower ℓ remains to be discussed. For a qualitative explanation compare also Fig. 3: Imagine l_N to be the smallest l for which at each instant $r > r_{\text{switch}}$. For this impact in both the approach and rebound phases the same Coulomb force, Bass potential, and friction force due to tunnelling act. However, for $l = l_N - l$ one crosses $r = r_{\text{switch}}$, i.e., a neck appears and although the dynamics in the approach phase is completely the same as for l_N , the rebound phase is essentially different (surface force instead of Bass force, another Coulomb force another bulk force). Thus, quasielastic and deep inelastic collisions are not uniquely treated in the model.

4. PARAMETER VARIATIONS

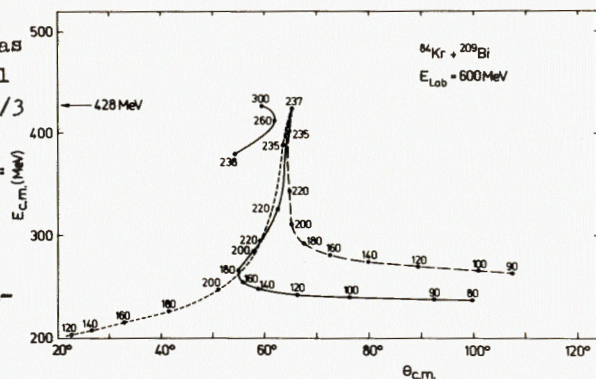
Since the bulk and surface forces are essentially determined by the evolution of the neck connecting the colliding ions, the dependence of model predictions with respect to variations of the parameters α and β should be studied more in detail. In particular, the question arises whether the values $\alpha = 0.04 \text{ fm/c}$ and $\beta = 1/3$ resulting from a fit to the TDHF results of ^{16/} for the $^{208}\text{Pb} + ^{208}\text{Pb}$, $E_{\text{c.m.}} = 800 \text{ MeV}$ reaction at zero impact can be used as standards over a wide range of projectile-target combinations, incident energies and impact parameters.

Table 1: Final c.m. energy, maximum neck radius, distance of closest approach, distance at which scission occurs, and interaction time for several combinations of α and β (eqs.(11),(12)) in the reaction $^{208}\text{Pb} + ^{208}\text{Pb}$ at $E_{\text{c.m.}} = 800 \text{ MeV}$, $L = 0$

	1 (standard)	2	3	4	5
α (fm/c)	0.04	0.02	0.08	0.04	0.04
β	1/3	1/3	1/3	0.4	0.25
final E c.m. (MeV)	520.6	550.4	483.0	575.3	418.0
$r_{\text{neck}}^{\text{max}}$ (fm)	4.52	4.32	4.74	4.52	4.52
r_{min} (fm)	12.18	12.1	12.29	12.18	12.18
r_{sci} (fm)	22.7	21.9	23.4	21.0	26.2
$\tilde{\tau}$ (10^{-21} s)	1.48	1.37	1.6	1.27	2.09

In table 1 several dynamical quantities for 5 sets of parameters α , β are quoted for the reaction $^{208}\text{Pb} + ^{208}\text{Pb}$, $L = 0$, $E_{\text{c.m.}} = 800 \text{ MeV}$. By comparing the second and third column with the first one (standard values) it is seen that for a fixed β even a change of α by a factor of two has only a quite small consequence on the evolution of the neck in the approach phase (maximum neck radius $r_{\text{neck}}^{\text{max}}$, closest distance of the ions r_{min}) while changes of 30-40 MeV in the final c.m. energy result. Thus, even small uncertainties

Fig.5. Wilczynski plot for the same reaction as in Fig.4. Bertsch model predictions for $\beta = 1/3$ (full line), $\beta = 0.4$ (long-dashed line), $\beta = 0.25$ (short-dashed line), the remaining parameters taken to be the corresponding standard ones. The numbers near the curves denote the initial angular momentum in units of \hbar .



in the determination of the geometric neck characteristics in the approach phase from TDHF can lead to substantial uncertainties in the parameter α , which in turn have appreciable consequences for the total energy loss during the whole reaction.

An even more drastic effect results from 25% variations of β (for fixed standard α). Fortunately, the distance r_{sci} between the ions when scission happens is sufficiently sensitive to β and so its extraction from TDHF is less ambiguous. Nevertheless, TDHF evolutions for different systems should yield somewhat different values for the parameter β . So, it is interesting to compare model predictions for the parameter values of columns 4 and 5. The corresponding Wilczynski plots for the same reaction as in Fig. 4 are shown in Fig. 5. There are quite large deviations for medium and low impact parameters. In this context it would be interesting to derive "best fit" parameters α and β from the TDHF calculations for various systems in order to get a feeling of whether there exists an over-all set of values α , β which can be used for any system or not.

Various TDHF calculations (compare, e.g. ^{19/}) indicate that in the neck region the central density is somewhat smaller than ρ_0 and the diffuseness of the surface is larger than in static nuclei. Correspondingly, charge density in the neck ρ_n and surface tension σ should effectively be somewhat overestimated in the Bertsch model.

This should most clearly be seen for very large systems (the Coulomb force to be essential enough) which (at least in TDHF) fuse in some region of impact parameters. Then, the critical l for fusion should strongly depend on effective changes in the surface force (i.e. σ). We have performed model calculations for the reaction $^{208}\text{Pb} + ^{74}\text{Ge}$, $E_{lab}(\text{Pb}) = 1600$ MeV and plotted energy losses and deflection angles as functions of orbital momentum in Fig.6.

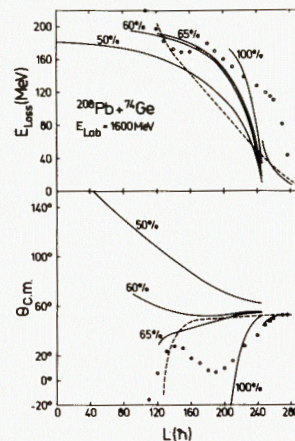


Fig. 6.

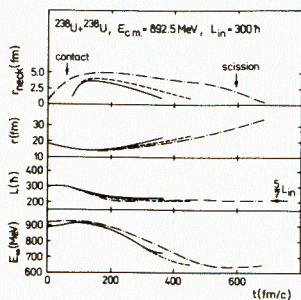
Energy loss and deflection angle for the $^{208}\text{Pb} + ^{74}\text{Ge}$, $E_{Lab}(\text{Pb}) = 1600$ MeV reaction as functions of initial angular momentum in comparison with TDHF^{11/} (circles) and a model prediction of ref.^{12/} (dashed lines). The present Bertsch model calculations (full lines) are shown for the standard value $\sigma = 1 \text{ MeV/fm}^2$ (100%) as well as for 50, 60, 65% of it.

For this system a recent TDHF calculation^{11/} predicts fusion (capture, leading to $^{282}114^*$) below $l_{crit} = 110 \hbar$ while the Bertsch model yields fusion even for $l \approx 205 \hbar$. We relate this to an overestimation of the (attractive) surface force and repeated the calculation for smaller values of σ and Z_n in eqs. (2) and (9). In Fig.6 we included results for 65%, 60% and 50% of the standard values ($\sigma = 1 \frac{\text{MeV}}{\text{fm}^2}$). While the reduction of Z_n was found to have a minor effect the lowering of σ drastically changed the picture. In the last case no fusion occurs at all, and forward scattering turns out to be possible only for grazing collisions. The first case, however, comes close to TDHF predicting a value of $l_{crit} = 121 \hbar$. While with decreasing surface tension the fusion region smoothly decreases, we have obtained negative forward angles (onset of orbiting) only for $\sigma \approx 0.75 \text{ MeV/fm}^2$. For σ values of about 0.6 MeV/fm^2 the deflection function shows a pronounced focussing behaviour as in a recent model calculation of ref. ^{12/} in the framework of an extended phenomenological surface friction model^{13/}, which allows for independent dynamical deformations of the two ions, for fluctuations in re-

lative motion and deformation degrees of freedom as well as for charge and mass transfer ^{/14/}. For $\zeta = 0.65 \text{ MeV/fm}^2$ ($\approx 65\%$) the energy loss predictions of TDHF are also reproduced quite well, except near grazing collisions for which both classical models yield a substantial underestimation. Bertsch^{/1/} related this general disadvantage of the model to the neglect of deformation degrees of freedom before the nuclei touch, which are important for absorbing energy in grazing trajectories^{/15/}. The present results indicate that TDHF shows a tendency of decreasing surface tension in very diffuse large necks with central density somewhat smaller than ρ_0 . On the other hand, owing to the facts that superheavy elements have not yet been found in experiments, and the inclusion of residual two-body interactions would only increase the capture cross section, one can conclude that TDHF nevertheless slightly (10-15%) overestimates surface tension in such exotic systems. If so, the appearance of fusion (capture) leading to superheavies in TDHF could be an artifact of the theory resulting from effective nucleon-nucleon forces deduced from bulk properties (e.g., surface energy) of static nuclei.

Finally, we consider the memory time t_0 which is not unambiguously fixed in the model. In one-dimensional slab dynamics it turns out to be twice t_0 ^{/8/}. On the other hand it would be equal to t_0 if the far surfaces of the nuclei move with the velocities of their centers of mass. However, there will also be some delay in the motion of the far surfaces with respect to the mass centers. Therefore, in^{/1/} the value of eq. (8) was chosen as a standard one. In order to estimate the dependence of model predictions on variations of t_0 we have performed calculations for the reaction presented in Fig.2 with $t_D = 1.5 t_0$ as well as with $t_D = 0.9 t_0$.

Fig.7.



Time evolution of neck radius r_{neck} , separation distance r , orbital angular momentum L , and the total c.m. kinetic energy projected to infinite separation E_{∞} , for the reaction presented in Fig.2. Full lines: $t_D = 1.5 t_0$. Dashed lines: $t_D = 0.9 t_0$. Dotted-dashed lines: TDHFB predictions, taken from ref. ^{/16/}. For clearness the TDHFB curve for E_{∞} is shifted upwards by 30 MeV.

In Fig.7 corresponding results are shown in comparison with TDHFB predictions of ^{/16/}. While in the standard version the neck radius, interaction time and the final energy loss $E_{c.m.}(t=0) - E_{\infty}(t \rightarrow \infty)$ are somewhat underestimated, the predictions for the smaller value come closer to TDHFB. This is because a larger memory time implies that the system bounces more elastically ^{/1/}. The final total angular momentum only slightly depends on the choice of t_D . In both cases, as in TDHFB, a rapid approach to equilibrium occurs. While for $t_D = 1.5 t_0$ the rigid clutching value is not quite reached, the equilibrium L value for $t_D = 0.9 t_0$ is even somewhat smaller. This is connected with the use of moments of inertia for rigid ellipsoids in eq. (5) instead of those of rigid spheres. Although we found that a decrease of t_D improves the agreement with mean-field predictions it does not necessarily mean that a memory time smaller than the standard value should be used in the model since there are some more effects in the same direction as discussed above.

5. COMPARISON WITH OTHER MODELS AND EXPERIMENTAL DATA

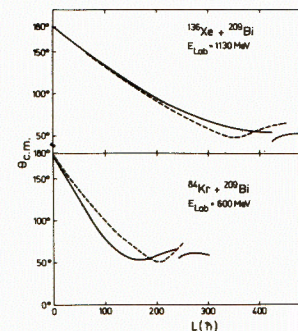
Since the Bertsch model heavily relies on the nucleon fluxes across the neck as well as on different deformations in the entrance / exit channels to be the basic mechanisms of relative-motion - energy loss, it is of interest to compare it with other classical models which also use a soft (proximity) friction ^{/2/} and include some simulation of the neck evolution (i.e. deformations).

As an example, we compare with predictions of ref. ^{/17/} for the $^{136}\text{Xe} + ^{209}\text{Bi}$, $E_{\text{lab}} = 1130 \text{ MeV}$ and $^{84}\text{Kr} + ^{209}\text{Bi}$, $E_{\text{lab}} = 600 \text{ MeV}$ reactions. In that model the ions are allowed to have growing prolate deformations in the exit channel.

Fig.8.

Deflection angle as a function of initial orbital angular momentum for the $^{136}\text{Xe} + ^{209}\text{Bi}$ and $^{84}\text{Kr} + ^{209}\text{Bi}$ reactions at $E_{\text{lab}} = 1130 \text{ MeV}$ and 600 MeV , respectively. Full lines: present Bertsch model calculations.

Dashed lines: model predictions taken from ref. ^{/17/}. For details see text.



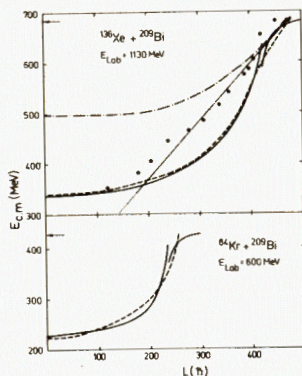


Fig. 9.

Final kinetic energy as a function of initial orbital momentum for the same reactions as in Fig.8. Full and dashed lines have the same meaning as in Fig.8. Dotted-dashed line: model prediction of ref. /17/ without deformation. Dotted line and full circles: results of experimental analyses of refs. /19/ and /20/, respectively.

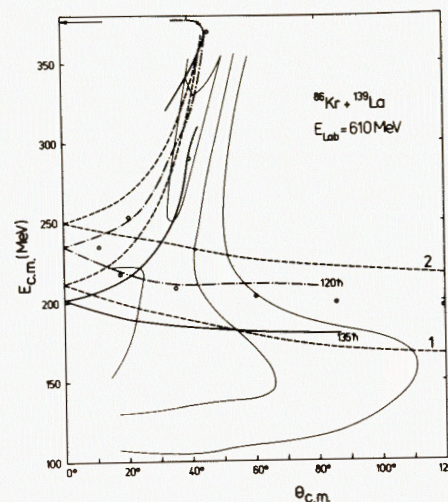
The use of the proximity potential /18/ and one-body dissipation leaves no room for free parameters. Particle transfer and thermal fluctuations are also included opposite to the Bertsch model. They should, however, have no substantial influence on the first moments of deflection angles and final kinetic energies shown in Figs.8 and 9 as functions of initial orbital momentum. A good agreement between both model predictions can be stated. There are, however, some deviations in the $^{84}\text{Kr} + ^{209}\text{Bi}$ case where the Bertsch model yields more forward angles and larger energy losses for intermediate impacts. Seemingly, in this case the surface force in the Bertsch model, connected with an energy loss, has a larger effect than that of different proximity potentials in the entrance (spheres) and exit (prolate deformations) channels in ref. /17/. Energy losses resulting from experimental analyses of refs. /19,20/ are also shown in Fig.9. Although, the experimental data seem to indicate too large damping for intermediate L in both models, a comparison with the experimental energy - angular correlations /20/ (see Fig.11) shows that the Bertsch model gives good average agreement with the experimental cross sections. This discrepancy arises from the presence of large spreads in the final energy and angular momentum of the fragments.

For further comparison, calculations of /17/ without deformation are also included in Fig. 9. It is clearly seen that trajectory calculations completely fail in this case and cannot reproduce the observed energy loss.

We now wish compare the Bertsch model with a classical model which uses folding potential and steep friction form factors (surface friction) in the spirit of ref. /21/ and which also includes de-

formation. To this aim we choose the model of ref. /14/ (see also discussion to Fig.6) which allows for independent quadrupole deformations of both ions.

Fig.10.



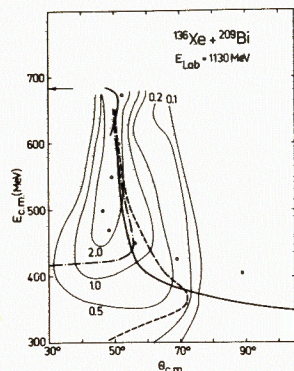
Wilczynski plot for the $^{86}\text{Kr} + ^{139}\text{La}$, $E_{\text{Lab}} = 610 \text{ MeV}$ reaction. Experimental data (thin lines) are taken from ref. /22/. Dashed lines: model predictions of ref. /14/ with (1) and without (2) deformation. Thick full line: present Bertsch model predictions. Circles: TDHF predictions of ref. /23/. Dotted-dashed line: model prediction of ref. /25/ (time-dependent nuclear potential but no deformation). For details see text.

In Fig. 10 the corresponding results with and without deformation are compared with the Bertsch model prediction and experimental double-differential cross sections /22/. The influence of the deformation is qualitatively similar as in the case of Fig. 9. The results of ref. /14/ with deformation are quite close to the present calculations. They are both closer to the averaged experimental values than TDHF predictions of ref. /23/. Because of the phenomenological character of the Bertsch model it is hard to find a reasonable explanation for the energy losses to be larger than in TDHF, all the more since in other cases (compare, e.g., Fig.4,7) we got opposite tendencies. A similar good description of the reaction under consideration has been reported in ref. /24/ using another version of the surface friction + deformation model.

It is interesting to note that seemingly part of the additional energy loss due to deformation can already be simulated by using different nuclear potentials in the approach and rebound phase for spherical nuclei. This can be seen from a comparison with a model calculation of ref. /25/ (Fig.10) which uses a surface friction force and a time-dependent nuclear potential, smoothly switching

over from a diabatic (proximity) to an adiabatic (Woods-Saxon-type) potential in a characteristic time of about 10^{-21} s. In both the Bertsch model and that of ref. /14/ different deformations in the entrance and exit channel course a corresponding asymmetry not only in the nuclear force but also in the friction force. Thus, the energy losses are still larger.

Fig.11.



Wilczynski plot for the $^{136}\text{Xe} + ^{209}\text{Bi}$, $E_{\text{Lab}} = 1130$ MeV reaction. Experimental data (thin lines) are taken from ref. /20/. Dashed and dott-dashed lines: model predictions of ref. /14/ with and without deformation, respectively. Circles: TDHF predictions of ref. /26/. Full line: present Bertsch model calculation with continuous bulk force.

While the Kr + La reaction considered above is typical for orbiting reactions, it is of interest to look for a reaction with completely different angular behaviour, e.g., a focusing reaction like $^{136}\text{Xe} + ^{209}\text{Bi}$, $E_{\text{lab}} = 1130$ MeV. Fig.11 shows a comparison between predictions of ref. /14/ with and without quadrupole deformations (see discussion to Fig.10), Bertsch model predictions, TDHF results of ref. /26/, and experimental energy-angular correlations (Wilczynski plots) /20/. Since in Figs. 8, 9 the results for the same reaction using the standard version are already shown, we plot here the modified version described in sect. 3. Concerning the results of /14/ we state that because deformation absorbs energy out of both radial and tangential relative motion it again leads to higher energy losses as well as to larger deflection angles (for comparable interaction times). Our results quite well agree with those of /14/ at large and intermediate impacts. However, for violent collisions we got a smooth increase of the deflection angle while a quadrupole deformation yields a decrease of the deflection angle for smallest L , i.e., a tendency to orbiting. It is hard to interpret this discrepancy between two quite different phenomenological models. However, one cannot exclude that this different angle behaviour gives us a hint that at small impact parameters besides quadrupole deformation higher multipolarities come into play. To some extent they are

included in the Bertsch model since a multipole expansion of the neck would give nonzero contributions for higher order deformations, the dynamics of which is, however, not explicitly described and somewhat artificially constraint by the geometry chosen in the model.

6. CONCLUSIONS

We have performed a detailed investigation of Bertsch's classical model for heavy ion collisions based on the known bulk dynamics of mean-field theory. The main qualitative feature of this model is that the bulk force connected with particle transfer has some non-dissipative character due to memory effects while the potential interaction includes a surface force which gives a contribution to the energy loss originating from different shapes in the approach and rebound phases.

The qualitative agreement with TDHF and more or less involved phenomenological models (each including deformations) as well as with experimental data is encouraging. Some quantitative deviations from experimental data and/or TDHF predictions can be removed to a large extent if the parameters of the model, which in the standard version are obviously chosen suitably, are considered as adjustable ones without having physically motivated regions of variation.

Further theoretical work should be done in the direction of motivating different parameter choices (or even calculating them in a more involved framework) as well as of including mass transfer and statistical spreadings of observable quantities in order to get double-differential cross sections directly comparable with experiments.

Starting from a reasonable description of the trajectories, neck development and particle fluxes between the ions, it is also possible to set up a sufficiently simple but physically well motivated model for particle emission at low and intermediate ($\lesssim 20$ MeV/A) incident energies /27/.

REFERENCES

1. Bertsch G.F. Preprint MSUCL- 385, Michigan, 1982.
2. Randrup J. Ann. of Phys., 1978, 112, p.356.
3. Jain A., Sarma N. Phys. Rev. C, 1981, 24, p. 1066.

4. Bass R. Phys. Rev. Lett., 1977, 39, p. 265.
5. Ko C.M., Bertsch G.F., Cha D. Phys. Lett. B, 1978, 77 p.174.
6. Dhar A.K., Nilsson B. Phys.Lett.B,1978,77,p. 50.
7. Rayleigh J. Collected Scientific Papers, Vol. 1, Dover, 1964,p.361
8. Bertsch G.F., Munding D. Phys.Rev.C, 1978, 17,p. 1646.
9. Davies K.T.R., Koonin S.E. Phys. Rev. C, 1981, 23, p. 2042.
10. Devi K.R.S. et al. Phys.Rev.C, 1981, p.1064.
11. Dhar A.K. Phys. Rev.Lett., 1983, 50, p. 478.
12. Fröbrich P. Phys. Rev.C. 1984,29, p. 338.
13. Fröbrich P. Phys. Lett. B, 1983, 122, p.338.
14. Fröbrich P., Strack B., Durand M. Nucl.Phys.A, 1983, 406,p.557.
15. Broglia R.A. et al. Phys.Lett.B, 1976, 61,p.113.
16. Cusson R.Y., Maruhn J.A., Stöcker H. Z. Phys. A, 1980, 294,p.257.
17. Samaddar S.K. et al. Physica Scripta, 1981, 23,p. 231.
18. Blocki J. et al. Ann.of Phys., 1977, 105, p. 427.
19. Huizenga J.R. et al. Phys. Rev. Lett., 1976, 37, p.885.
20. Schröder W.V. et al. Phys.Rep., 1978, 45,p.301.
21. Gross D.H.E., Kalinowski H. Phys. Rep., 1978, 45,p.175.
22. Vandenbosch R. et al. Phys.Rev.C, 1978, 17, p. 1672.
23. Davies K.T.R., Devi K.R.S., Strayer M.R. Phys. Rev. C, 1979,20 p. 1372.
24. Blocki J. et al. Phys.Lett. B, 1981, 99, p. 13.
25. Gnucci C., Stanev Fl. Nucl. Phys. A, 1981, 366, p. 520.
26. Dhar A.K. et al. Nucl. Phys.A, 1981, 364, p. 105.
27. Biedermann M., Mädler P., Reif R. in preparation.

SUBJECT CATEGORIES OF THE JINR PUBLICATIONS

Index	Subject
1.	High energy experimental physics
2.	High energy theoretical physics
3.	Low energy experimental physics
4.	Low energy theoretical physics
5.	Mathematics
6.	Nuclear spectroscopy and radiochemistry
7.	Heavy ion physics
8.	Cryogenics
9.	Accelerators
10.	Automatization of data processing
11.	Computing mathematics and technique
12.	Chemistry
13.	Experimental techniques and methods
14.	Solid state physics. Liquids
15.	Experimental physics of nuclear reactions at low energies
16.	Health physics. Shieldings
17.	Theory of condensed matter
18.	Applied researches
19.	Biophysics

Received by Publishing Department
on June 18, 1984.

WILL YOU FILL BLANK SPACES IN YOUR LIBRARY?

You can receive by post the books listed below. Prices - in US \$,
including the packing and registered postage

	Proceedings of the VII All-Union Conference on Charged Particle Accelerators. Dubna, 1980. 2 volumes.	25.00
	Proceedings of the VIII All-Union Conference on Charged Particle Accelerators. Protvino, 1982. 2 volumes.	25.00
D2-81-543	Proceedings of the VI International Conference on the Problems of Quantum Field Theory. Alushta, 1981	9.50
D1,2-81-728	Proceedings of the VI International Seminar on High Energy Physics Problems. Dubna, 1981.	9.50
D17-81-758	Proceedings of the II International Symposium on Selected Problems in Statistical Mechanics. Dubna, 1981.	15.50
D1,2-82-27	Proceedings of the International Symposium on Polarization Phenomena in High Energy Physics. Dubna, 1981.	9.00
D2-82-568	Proceedings of the Meeting on Investigations in the Field of Relativistic Nuclear Physics. Dubna, 1982	7.50
D3,4-82-704	Proceedings of the IV International School on Neutron Physics. Dubna, 1982	12.00
D11-83-511	Proceedings of the Conference on Systems and Techniques of Analytical Computing and Their Applications in Theoretical Physics. Dubna, 1982.	9.50
D7-83-644	Proceedings of the International School-Seminar on Heavy Ion Physics. Alushta, 1983.	11.30
D2,13-83-689	Proceedings of the Workshop on Radiation Problems and Gravitational Wave Detection. Dubna, 1983.	6.00
D13-84-63	Proceedings of the XI International Symposium on Nuclear Electronics. Bratislava, Czechoslovakia, 1983.	12.00
E1,2-84-160	Proceedings of the 1983 JINR-CERN School of Physics. Tabor, Czechoslovakia, 1983.	6.50

Orders for the above-mentioned books can be sent at the address:
Publishing Department, JINR
Head Post Office, P.O.Box 79 101000 Moscow, USSR

Бидерман М., Мэдлер П., Райф Р. E7-84-415
Макроскопическая модель для столкновения тяжелых ионов,
мотивированная самосогласованными расчетами:
сравнительный анализ

Детально изучена классическая модель Берча для описания столкновений тяжелых ионов, основывающаяся на главных чертах приближения, зависящего от времени Хартри-Фока /ЗВХФ/. Эта модель хорошо согласуется с ЗВХФ и феноменологическими моделями, учитывающими степени свободы, связанные с деформацией, а также с экспериментальными данными. Некоторые количественные отклонения от эксперимента и/или ЗВХФ в большой мере могут быть устранены, если рассматривать стандартные параметры модели как подгоночные в физически разумных пределах вариации.

Работа выполнена в Лаборатории теоретической физики ОИЯИ.

Сообщение Объединенного института ядерных исследований. Дубна 1984

Biedermann M., Mädler P., Reif R. E7-84-415
TDHF-Motivated Macroscopic Model for Heavy Ion
Collisions: A Comparative Study

A detailed investigation of Bertsch's classical TDHF-motivated model for the description of heavy ion collisions is performed. The model agrees well with TDHF and phenomenological models which include deformation degrees of freedom as well as with experimental data. Some quantitative deviations from experiment and/or TDHF can be removed to a large extent if the standard model parameters are considered as adjustable parameters in physically reasonable regions of variation.

The investigation has been performed at the Laboratory of Theoretical Physics, JINR.

Communication of the Joint Institute for Nuclear Research. Dubna 1984